Acta Crystallographica Section F
Structural Biology and Crystallization Communications
ISSN 1744-3091

Production, purification and preliminary X-ray crystallographic studies of adeno-associated virus serotype 1

Edward B. Miller,[a] Brittney Gurda-Whitaker,[a] Lakshmanan Govindasamy,[a] Robert McKenna,[a] Sergei Zolotukhin,[b] Nicholas Muzyczka[c] and Mavis Agbandje-McKenna[a]*

[a]Department of Biochemistry and Molecular Biology, College of Medicine, University of Florida, Gainesville, FL 32610, USA, [b]Department of Pediatrics, College of Medicine, University of Florida, Gainesville, FL 32610, USA, and [c]Department of Molecular Genetics and Microbiology, College of Medicine, University of Florida, Gainesville, FL 32610, USA

Correspondence e-mail: mckenna@ufl.edu

Received 10 September 2006
Accepted 12 November 2006

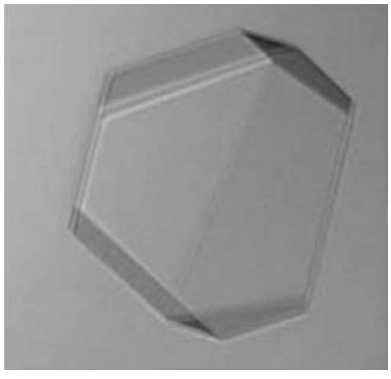

Crystals of baculovirus-expressed adeno-associated virus serotype 1 (AAV1) capsids have been grown in the rhombohedral space group *R*32 (unit-cell parameters $a = 254.7$ Å, $\alpha = 62.3^\circ$) and shown to diffract X-rays to at least 2.5 Å resolution. The diffraction data were subsequently processed and reduced with an overall R_{sym} of 12.3% and a completeness of 89.0%. Based on the unit-cell volume, rotation-function and translation-function results and packing considerations, there is one virus capsid (60 viral proteins) per unit cell and there are ten viral proteins per crystallographic asymmetric unit. The AAV1 capsid shares both the twofold and threefold crystallographic symmetry operators. The AAV1 data have been initially phased using a polyalanine model (based on the crystal structure of AAV4) to 4.0 Å resolution and the structure determination and refinement is in progress using tenfold noncrystallographic symmetry electron-density averaging.

1. Introduction

The adeno-associated viruses (AAVs) are members of the *Parvoviridae* family that are classified under the genus *Dependovirus* (Muzyczka & Berns, 2001). The AAVs are small $T = 1$ icosahedral ssDNA viruses with a mean diameter of 260 Å. Several AAV serotypes have been isolated from humans, nonhuman primates and other mammals (reviewed by Bowles *et al.*, 2006). These viruses are nonpathogenic and recombinant forms can transduce human tissue for corrective gene-delivery applications (Kotin, 1994). Clinical trials using the AAVs have included gene delivery for the treatment of cystic fibrosis, hemophilia and muscular dystrophy (reviewed by Carter, 2006).

AAV capsids are composed of three overlapping capsid viral proteins (VPs) identified as VP1, VP2 and VP3 of 87, 73 and 62 kDa, respectively. These VPs are present in the capsids in a ratio of 1:1:10, respectively, with VP1 and VP2 having N-terminal extensions compared with VP3. The structures of three AAV serotypes (AAV2, AAV4 and AAV5) have been determined by X-ray crystallography and/or cryo-electron microscopy and image reconstruction (Xie *et al.*, 2002; Walters *et al.*, 2004; Padron *et al.*, 2005; Govindasamy *et al.*, 2006). Only the VP3 common region of the VPs is observed in the structures, with 60 copies forming the $T = 1$ icosahedral capsid.

The AAV serotypes exhibit dramatic differences in cell tropism and *in vivo* tissue transduction (Gao *et al.*, 2004). For example, AAV1 is able to transduce muscle cells much more efficiently than AAV2 (the best characterized serotype) and several of the other serotypes (Xiao *et al.*, 1999; Chao *et al.*, 2000; Gao *et al.*, 2004). A small number of amino-acid differences in the overlapping VP3 region dictate the recognition of different cell-surface glycans and therefore the differential tropism and transduction properties of the AAVs (Opie *et al.*, 2003; Kern *et al.*, 2003; Wu, Azokan *et al.*, 2006). For example, AAV2 utilizes heparin sulfate as a primary receptor for cellular transduction, while AAV1 infection is facilitated by binding to terminal sialic acid (Summerford & Samulski, 1998; Wu, Miller *et al.*, 2006).

Here, we report the production, purification, crystallization and preliminary crystallographic analysis of the AAV1 capsid. The goal is to structurally characterize the capsid regions responsible for differ-

ences in tissue tropism, receptor binding and transduction efficiency between the AAV serotypes.

2. Materials and methods

2.1. Production and purification

Recombinant AAV1 capsids were produced using the Bac-to-Bac baculovirus expression system (Gibco BRL) with a construct able to express VP1, VP2 and VP3 as previously described for AAV5 (DiMattia *et al.*, 2005). A titered baculovirus stock was used to infect Sf9 insect cells grown in Erlenmeyer flasks at 300 K using Sf-900 II SFM media (Gibco/Invitrogen Corporation). The cells were infected at a multiplicity of infection of 5.0 plaque-forming units per cell.

The virus capsids were released from infected cells by three cycles of rapid freeze–thaw in lysis buffer (50 m*M* Tris–HCl pH 8.0, 100 m*M* NaCl, 1 m*M* EDTA, 0.2% Triton X-100), with the addition of benzonase (Merck KGaA, Germany) after the second cycle. The sample was clarified by centrifugation at 12 100*g* for 15 min at 277 K. The cell lysate was pelleted through a 20%(*w*/*v*) sucrose cushion (in 25 m*M* Tris–HCl pH 8.0, 0.3% Triton X-100, 100 m*M* NaCl; buffer *A*) by ultracentrifugation at 149 000*g* for 3 h at 277 K. The pellet from the cushion was resuspended in buffer *A* overnight at 277 K. The sample was further subjected to multiple low-speed spins at 10 000*g* in order to remove insoluble material. The clarified sample was loaded onto a sucrose-step gradient [10–40%(*w*/*v*)] and spun at 151 000*g* for 3 h at 277 K. A visible blue virus-capsid band in the 20% sucrose layer was extracted and dialyzed into 50 m*M* Tris–HCl pH 8.0, 15 m*M* NaCl at 277 K. The approximate concentration of the sample was calculated from optical density measurements at 280 nm, assuming an extinction coefficient of 1.7 for calculations in mg ml^{-1}. The purity and integrity of the viral capsids were monitored using SDS–gel electrophoresis and negative-stain electron microscopy, respectively. The sample was buffer-exchanged at 5000*g* using Amicon Ultra filters (Amicon Ultra-15, 10 kDa molecular-weight cutoff, Millipore Corporation) into 100 m*M* HEPES–NaOH pH 7.3, 50 m*M* $MgCl_2$, 0.03% NaN_3 and 25% glycerol with a final concentration of ∼10 mg ml^{-1}.

2.2. Electron microscopy

Purified capsids were viewed using a Joel JEM-100CX II electron microscope (EM). 4 µl purified capsids at an estimated concentration of 1.0 mg ml^{-1} was spotted onto a 400 mesh carbon-coated copper grid (Ted Pella Inc., Redding, CA, USA) for 1 min and blotted with filter paper (Whatman No. 5). The sample was then negatively stained with 4 µl 2% uranyl acetate for 15 s, blotted dry and viewed with the EM.

2.3. Crystallization

Screening for crystallization conditions utilized the hanging-drop vapor-diffusion method (McPherson, 1982) with VDX 24-well plates and siliconized cover slips (Hampton Research, Laguna Niguel, CA, USA). The crystallization screens were based on the published AAV2 crystallization conditions (Xie *et al.*, 2004), but with varying concentrations of NaCl (0.25–1.0 *M*) and PEG 6K (2–7%), drop size (4–14 µl) and the ratio of sample to precipitant solution in the drop (1:4 to 4:1). The hanging drops were suspended over 1.0 ml reservoir (precipitant) solution.

2.4. Data collection and reduction

Crystals were manually selected and flash-cooled to 100 K in a liquid-nitrogen stream prior to data collection. Additional cryoprotectant solution was not necessary as the crystals were grown in the presence of 25% glycerol. X-ray diffraction images were collected at the Advanced Photon Source (APS), Argonne National Laboratory on beamline 22-ID with a wavelength of 1.0 Å using a MAR300 CCD detector. A crystal-to-detector distance of 400 mm was used to record 0.3° oscillation images with an exposure time of 5 s per image. Observed diffraction intensities were indexed, integrated, scaled and merged using the *HKL*-2000 suite of programs (Otwinowski & Minor, 1997).

2.5. Molecular replacement: calculation of particle orientation and position

The orientation of the AAV1 viral capsid in the crystal unit cell was calculated with a self-rotation function using the *GLRF* program (Tong & Rossmann, 1997) using reflections between 10 and 4 Å resolution. The calculations used ∼10% of the largest amplitudes to represent the second Patterson. The radius of integration was set to 130 Å with κ = 72, 120 and 180° to search for fivefold, threefold and twofold noncrystallographic symmetry (NCS) elements of the icosahedral capsid, respectively. The molecular-replacement phasing procedure utilized the *CCP*4 program *AMoRe* (Navaza, 1994) with ten AAV4 VP3 polyalanine chains as a search model (PDB code 2g8g; Govindasamy *et al.*, 2006).

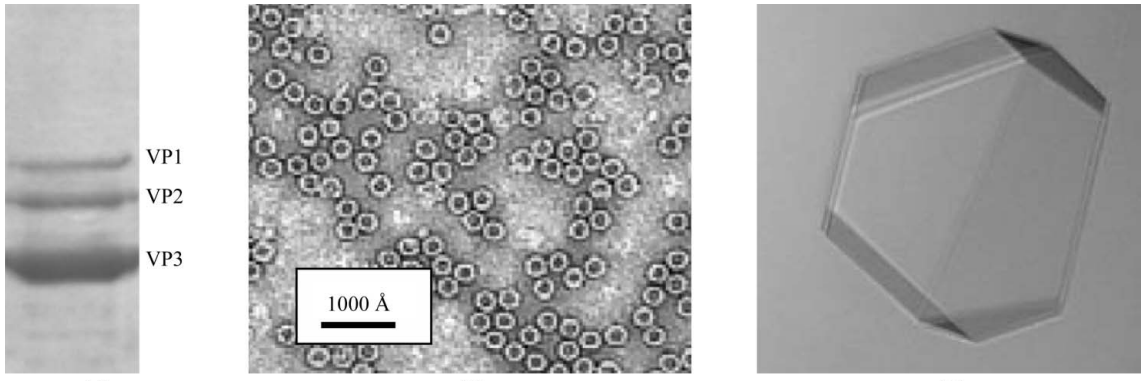

Figure 1
Purification and crystallization of AAV1 viral capsids. (*a*) SDS–PAGE gel depicting the relative ratio of the viral proteins VP1, VP2 and VP3 (molecular weights 87, 73 and 62 kDa, respectively). (*b*) Transmission electron micrograph of capsids stained with 2% uranyl acetate. (*c*) Optical photograph of an AAV1 capsid crystal. Approximate dimensions are 0.2 × 0.2 × 0.1 mm.

3. Results and discussion

3.1. Crystallization

The purity and integrity of the AAV1 capsids were confirmed with SDS–PAGE (Fig. 1*a*) and negative-stain EM (Fig. 1*b*) prior to crystallization.

AAV1 crystals grew at room temperature using a solution consisting of 0.1 *M* HEPES–NaOH pH 7.3, 0.05 *M* $MgCl_2$, 0.03% NaN_3, 0.25–1.0 *M* NaCl, 5–7% PEG 6K and 25% glycerol as the precipitant. At lower NaCl concentrations rapid nucleation was observed, resulting in small crystals, while lower percentages of PEG 6K at high salt concentrations did not yield any crystals. The crystals used for X-ray diffraction data collection were selected from conditions containing 1.0 *M* NaCl and 7% PEG 6K, with drop volumes of 4 or 8 µl and a sample:precipitant ratio of 1:1. These crystals were obtained in approximately two to three weeks and grew to dimensions of approximately 0.2 × 0.2 × 0.1 mm (Fig. 1*c*).

3.2. Data collection, processing and scaling

A total of 319 useful images were collected from six AAV1 crystals with an oscillation angle of 0.3°, providing a total of 95.7° of useable data. The crystals diffracted X-rays to at least 2.5 Å resolution. The images were indexed and the crystals were shown to belong to rhombohedral space group *R*32, with unit-cell parameters $a = 254.7$ Å, $\alpha = 62.3°$ and a unit cell volume of 13.16×10^6 Å^3. The mosaicity of the images ranged from 0.3 to 0.9°. A total of 962 546 observed reflections were reduced to 247 785 unique reflections with an overall R_{sym} of 12.3% and a completeness of 89.0%. Diffraction data were recorded beyond 2.5 Å resolution (2.1 Å resolution at the corners of the detector; Fig. 2), but owing to low completeness (<50%) the higher resolution reflections were not included in the data processing. The data-collection and processing statistics are given in Table 1.

3.3. Molecular replacement: particle orientation and position

A Matthews coefficient of 3.3 Å^3 Da^{-1} (62% solvent content) was calculated using the rhombohedral *R*32 unit-cell parameters and assuming the presence of one AAV1 capsid per unit cell (Matthews, 1968). This value was reasonable given the large hollow solvent volume in the interior of the empty (void of DNA) recombinant capsids. This observation was strongly suggestive that the AAV1 capsid was positioned on the *R*32 point-group crystal symmetry operation (with the $T = 1$ icosahedral capsid sharing both the twofold and threefold crystallographic symmetry operators), with ten VP monomers per crystallographic asymmetric unit.

Table 1
Data-collection and processing statistics.

Values in parentheses are for the highest resolution shell.

Space group	*R*32
Unit-cell parameters (Å, °)	$a = 254.7$, $\alpha = 62.3$
Unit-cell volume (Å^3)	13.16×10^6
V_M (Å^3 Da^{-1})	3.3
Total No. of reflections	962546
Unique reflections	247785
Crystal mosaicity (°)	0.3–0.9
Resolution range (Å)	50.0–2.5 (2.59–2.50)
Completeness (%)	89.0 (48.6)
R_{sym}†	0.123 (0.206)
Redundancy	3.9 (1.5)
Average $I/\sigma(I)$	12.3 (2.8)

† $R_{sym} = \sum |I_{hkl} - \langle I_{hkl}\rangle| / \sum |I_{hkl}|$, where I_{hkl} is the intensity of an individual *hkl* reflection and $\langle I_{hkl}\rangle$ is the mean intensity for all measured values of this reflection; the summation is over all equivalent intensities.

The data were transformed to the hexagonal setting *H*32 cell ($a = 262.7$, $c = 612.3$ Å) and the orientation of the AAV1 capsid was determined by a self-rotation function (Fig. 3). The results clearly showed that the icosahedral twofold and threefold axes were coincident with the crystallographic twofold (*a* axis) and threefold (*c** axis), respectively. The *c** axis in the hexagonal setting is equivalent to the body-diagonal threefold axis of the rhombohedral cell.

Based on these observations, the diffraction data were initially phased using molecular-replacement procedures with the *AMoRe* program. A decameric polyalanine VP3 model of AAV4 (which shares ∼59% sequence identity to AAV1) was orientated and positioned at (0, 0, 0) based on the crystal symmetry constraints. Using data to 4 Å resolution, the initial R_{work} and correlation coefficient were 46.1 and 56.8%, respectively.

The structure determination of the AAV1 capsid to 2.5 Å resolution using tenfold noncrystallographic symmetry electron-density averaging is currently in progress. Structural comparison of AAV1 with the crystal structures reported for AAV2 (Xie *et al.*, 2002) and AAV4 (Govindasamy *et al.*, 2006), combined with available mutagenesis and biochemical data (see, for example, Opie *et al.*, 2003;

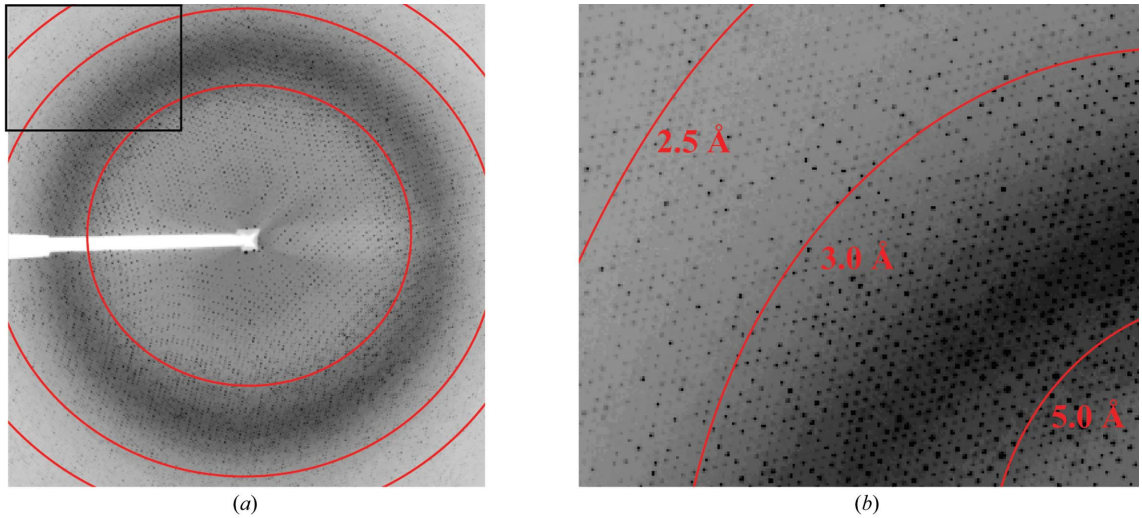

(*a*) (*b*)

Figure 2
X-ray diffraction image of an AAV1 crystal. (*a*) A typical 0.3° oscillation photograph. (*b*) Close-up view of the upper left-hand corner of (*a*). The concentric rings indicate the 5.0, 3.0 and 2.5 Å resolution shells, from right to left.

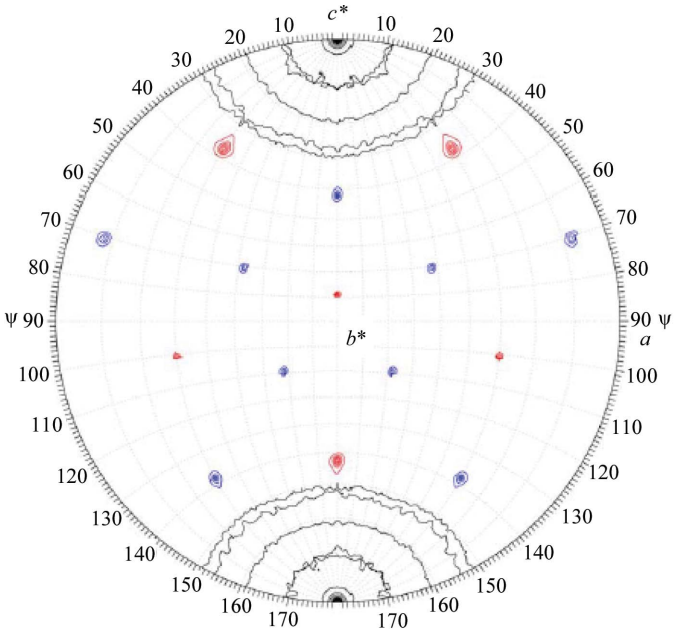

Figure 3
AAV1 viral capsid orientation in the *H*32 crystal setting. The self-rotation function is shown for κ = 72° (red) and 120° (blue), showing the fivefold and threefold icosahedral symmetry elements of the AAV1 capsid in the *H*32 unit cell. The search used observed data from 10.0 to 4.0 Å resolution, with a radius of integration of 130 Å. The rotation function is contoured at 2σ intervals.

Kern *et al.*, 2003; Wu, Asokan *et al.*, 2006; Wu, Miller *et al.*, 2006), will provide essential information for further analyzing the structural determinants of host range, receptor recognition and cellular transduction efficiencies for the AAV serotypes. The aim is to use this information to improve the efficacy of AAVs for specific cell/tissue-targeted gene-delivery applications.

The authors would like to thank the staff at the SER-CAT 22-ID beamline at APS, Argonne National Laboratory for assistance during X-ray diffraction data collection. We thank Dennifield Player (Anatomy and Cell Biology, University of Florida) for help with electron microscopy and Timothy Vaught (McKnight Brain Institute, Optical Microscopy Facility, University of Florida) for taking the optical photograph of the AAV1 crystals. We also thank Robert Kotin (National Heart, Lung and Blood Institute, Bethesda, MD) for kindly providing the AAV1 baculovirus construct. This project was funded by the Arnold and Mabel Beckman Foundation through the Beckman Scholars Program to EBM and NIH projects P01 HL59412 and P01 HL51811 to NM, SZ and MA-M.

References

Bowles, D. E., Rabinowitz, J. E. & Samulski, R. J. (2006). *Parvoviruses*, edited by J. R. Kerr, S. F. Cotmore, M. E. Bloom, R. M. Linden & C. R. Parrish, pp. 15–23. New York: Edward Arnold.
Carter, B. J. (2006). *Parvoviruses*, edited by J. R. Kerr, S. F. Cotmore, M. E. Bloom, R. M. Linden & C. R. Parrish, pp. 500–510. New York: Edward Arnold.
Chao, H., Liu, Y., Rabinowitz, J., Li, C., Samulski, R. J. & Walsh, C. E. (2000). *Mol. Ther.* **2**, 619–623.
DiMattia, M., Govindasamy, L., Levy, H. C., Gurda-Whitaker, B., Kalina, A., Kohlbrenner, E., Chiorini, J. A., McKenna, R., Muzyczka, N., Zolotukhin, S. & Agbandje-McKenna, M. (2005). *Acta Cryst.* F**61**, 917–921.
Gao, G. P., Vandenberghe, L. H., Alvira, M. R., Lu, Y., Calcedo, R., Zhou, X. & Wilson, J. M. (2004). *J. Virol.* **78**, 6381–6388.
Govindasamy, L., Padron, E., McKenna, R., Muzyczka, N., Kaludov, N., Chiorini, J. A. & Agbandje-McKenna, M. (2006). *J. Virol.* **80**, 11556–11570.
Kern, A., Schmidt, K., Leder, C., Muller, O. J., Wobus, C. E., Bettinger, K., Von der Lieth, C. W., King, J. A. & Kleinschmidt, J. A. (2003). *J. Virol.* **77**, 11072–11081.
Kotin, R. M. (1994). *Hum. Gene Ther.* **5**, 793–801.
McPherson, A. (1982). *Preparation and Analysis of Protein Crystals*, 1st ed., pp. 96–99. New York: Wiley.
Matthews, B. W. (1968). *J. Mol. Biol.* **33**, 491–497.
Muzyczka, N. & Berns, K. I. (2001). *Fields Virology*, 4th ed., edited by D. M. Knipe & P. M. Howley, pp. 2327–2360. New York: Lippincott, Williams and Wilkins.
Navaza, J. (1994). *Acta Cryst.* A**50**, 157–163.
Opie, S. R., Warrington, K. H. Jr, Agbandje-McKenna, M., Zolotukhin, S. & Muzyczka, N. (2003). *J. Virol.* **77**, 6995–7006.
Otwinowski, Z. & Minor, W. (1997). *Methods Enzymol.* **276**, 307–326.
Padron, E., Bowman, V., Kaludov, N., Govindasamy, L., Levy, H. C., Nick, P., McKenna, R., Muzyczka, N., Chiorini, J. A., Baker, T. S. & Agbandje-McKenna, M. (2005). *J. Virol.* **79**, 5047–5058.
Summerford, C. & Samulski, R. J. (1998). *J. Virol.* **72**, 1438–1445.
Tong, L. & Rossmann, M. G. (1997). *Methods Enzymol.* **276**, 594–611.
Walters, R. W., Agbandje-McKenna, M., Bowman, V. D., Moninger, T. O., Olson, N. H., Seiler, M., Chiorini, J. A., Baker, T. S. & Zabner, J. (2004). *J. Virol.* **78**, 3361–3371.
Wu, Z., Asokan, A., Grieger, J. C., Govindasamy, L., Agbandje-McKenna, M. & Samulski, R. J. (2006). *J. Virol.* **80**, 11393–11397.
Wu, Z., Miller, E., Agbandje-McKenna, M. & Samulski, R. J. (2006). *J. Virol.* **80**, 9093–9103.
Xiao, W., Chirmule, N., Berta, S. C., McCullough, B., Gao, G. & Wilson, J. M. (1999). *J. Virol.* **73**, 3994–4003.
Xie, Q., Bu, W., Bhatia, S., Hare, J., Somasundaram, T., Azzi, A. & Chapman, M. S. (2002). *Proc. Natl Acad. Sci. USA*, **99**, 10405–10410.
Xie, Q., Hare, J., Turnigan, J. & Chapman, M. S. (2004). *J. Virol. Methods*, **122**, 17–27.